J Seismol (2020) 24:979–989
https://doi.org/10.1007/s10950-020-09914-7

ORIGINAL ARTICLE

An application of coherence-based method for earthquake detection and microseismic monitoring (Irpinia fault system, Southern Italy)

G. M. Adinolfi · M. Picozzi · S. Cesca · S. Heimann · A. Zollo

Received: 15 May 2019 / Accepted: 24 March 2020 / Published online: 23 May 2020

Abstract A coherence-based earthquake detection technique was applied to continuous (1 year) waveform data recorded along the Irpinia fault system (Southern Italy). The earthquake detection was performed using coherent P- and S-wave arrivals recorded by the dense seismic network operating in Irpinia and assuming a local velocity model. We applied a strategy to simultaneously detect and locate earthquakes and to discriminate among true and false detections using an automated and fast procedure, able to process 1 year of data in ~ 1.75 days. The final catalogue of automatically retrieved earthquakes shows a performance improvement with respect to the standard monitoring practices, with an increase in the number of detected small events of about a factor three with respect to the automatic Earth-worm Binder implemented in ISNet and decreases in completeness magnitude of almost half unit magnitude.

Keywords Microseismicity · Induced Seismicity · Seismic Monitoring · Earthquake Detection · Earthquake Location · Irpinia Fault System · 1980 Irpinia Earthquake

Electronic supplementary material The online version of this article (https://doi.org/10.1007/s10950-020-09914-7) contains supplementary material, which is available to authorized users.

G. M. Adinolfi (✉) · M. Picozzi · A. Zollo
Department of Physics "Ettore Pancini", University of Naples "Federico II", Naples, Italy
e-mail: guidomaria.adinolfi@unina.it

S. Cesca · S. Heimann
GFZ German Research Centre for Geosciences Potsdam, Potsdam, Germany

1 Introduction

Automated, fast and accurate methods for detection and location of microseismicity are nowadays increasingly in demand. Seismic hazard management and industrial applications related to underground operations, such as hydrocarbon exploitation or geothermal stimulation, require accurate and rapid earthquake monitoring with detection of small events and the creation of earthquake catalogues complete to low magnitudes ($Mc < 0$; Wassermann 1997; Ekstrom 2006; McMechan 1982; Gajewski and Tessmer 2005; Krüger and Ohrnberger 2005; Kao and Shan 2007; Rubinstein and Beroza 2007; Gharti et al. 2010; Maercklin et al. 2012). In recent years, different techniques capable of rapidly and automatically processing large datasets and/or continuous waveforms have been designed (see Cesca and Grigoli 2015 for a review). Among these, coherence-based methods have undergone a considerable development (Grigoli et al. 2018; Matos et al. 2016; Lopez-Comino et al. 2017). These methods (also called migration-based) consist in migration techniques, extensively adopted in applied geophysics, which use the full waveform information to detect and locate seismic events at the same time. Coherence-based approaches, hence, perform a time-shifting and stacking of characteristic functions computed on seismic traces recorded at different stations to identify and locate earthquakes inside a pre-defined spatial grid of potential source locations (Withers et al. 1999; Gharti et al. 2010; Grigoli et al. 2013; Zeng et al. 2014). The characteristic functions of selected wave packets recorded at different stations are delayed and

stacked to maximize images of signal coherence (called Global Image Function, GIF). Then, these GIF are used to detect earthquakes and provide estimates of their location. These methods offer several advantages: (1) no manual phase identification and picking is required, (2) high reliability using noisy data, (3) full automated and fast processing and 4) high detection rate.

It is worth mentioning that the discrimination between real and false earthquake detections represents a critical aspect in seismic monitoring applications, which obviously becomes particularly problematic when operating seismic networks are not dense enough with respect to small magnitude targets.

In coherence-based methods, the event detection performance is influenced by the selection of coherence thresholds above which events are detected. Lopez-Comino et al. (2017) have shown that decreasing the coherence threshold increases the number of detections and the chance to detect weaker events, but at the cost of increasing the false detection rate. It became, thus, a priority to design and to implement strategies facilitating the discrimination between real and false detections, so as to improve the performances of seismic monitoring (Adinolfi et al. 2019; Grigoli et al. 2013, 2018).

In this work, we present the application of a coherence-based detection and location method to 1-year of seismic data recorded at the near-fault observatory operating along the Irpinia fault zone in Southern Apennines (Italy), (i.e., the Irpinia Seismic Network, ISNet, Fig. 1). In particular, we have tested a multistep procedure for discriminating real against false detections, including implicit information about the detectability of the seismic network, and for locating earthquakes using the P- and S-wave contributions. We have evaluated the performance of the earthquake detector by comparing our results with the earthquake catalogue obtained by the automatic Earth-worm Binder implemented in ISNet and the manual catalogue.

2 Area of study and data

The Irpinia fault system is a complex, extensional fault structure area, characterized by high seismic potential and past destructive earthquakes (Fig. 1; DISS, version 3.2.1). On 23 November 1980, a M_s. 6.9 earthquake occurred along NW-SE striking faults with a complex rupture characterized by three main episodes occurred within seconds that caused about 3000 fatalities and severe damage (Bernard and Zollo 1989). Recently, a M_L 4.9 earthquake, the largest one since 1980, occurred on the April 3rd, 1996, within the epicentral area of the 1980 earthquake and showed a normal fault mechanism (Cocco et al. 1999).

The instrumentally recorded seismicity in the Irpinia region (Southern Italy) is distributed uniformly in the uppermost 15 km of the crust, with normal to normal-strike focal mechanisms, evidencing a NE-SW extension consistent with the regional stress field in the Southern Apennines (De Matteis et al. 2012; De Landro et al. 2015; Amoroso et al. 2017; Adinolfi et al. 2015). Seismicity frequently occurs in the form of microseismic sequences or swarms that last typically a few days with weak events characterized by low maximum magnitudes ($M < 3.3$).

The seismicity in this area has been monitored since 2005 by a near-fault seismic observatory, the Irpinia Seismic Network (ISNet, Fig. 1; Weber et al. 2007; Picozzi et al. 2019). ISNet is a dense seismic network composed of 32 stations, each equipped with a three-component ground acceleration and three-component velocity (short period or broadband) sensors. ISNet covers an area of about 100 km × 70 km, focused on the Campania-Lucania Apennines portion where the M_s 6.9, 1980 earthquake enucleated, and is operated by the Department of Physics of the University of Naples "Federico II".

This work focuses on continuous waveforms recorded during the year 2018, the last available complete year when this study has started, by three-component velocity meter sensors (1 Hz short-periods and 40s broad-bands sensors) with a sampling frequency of 125 Hz. Due to variations in operating condition of the seismic network during the year, the dataset is complete for a maximum number of operating seismic stations equal to 19.

Seismic monitoring at ISNet combines automatic and manual operations that are performed by the RISSCLab team (i.e., the University research unit in experimental and computational seismology, http://www.rissclab.unina.it/it/). Earthquakes are first automatically detected by the Earth-worm binder (Dietz 2002) and later manually revised. Moreover, daily continuous waveforms are visually inspected by the team to find potentially missed events. After the P- and S- wave manual picking, earthquakes are located by using a local velocity model (Matrullo et al. 2013) and HYPOINVERSE2000 arrival time inversion program (Klein 2003). The hypocentre parameters and (moment and local) magnitudes for the earthquakes inside the network are reported on the

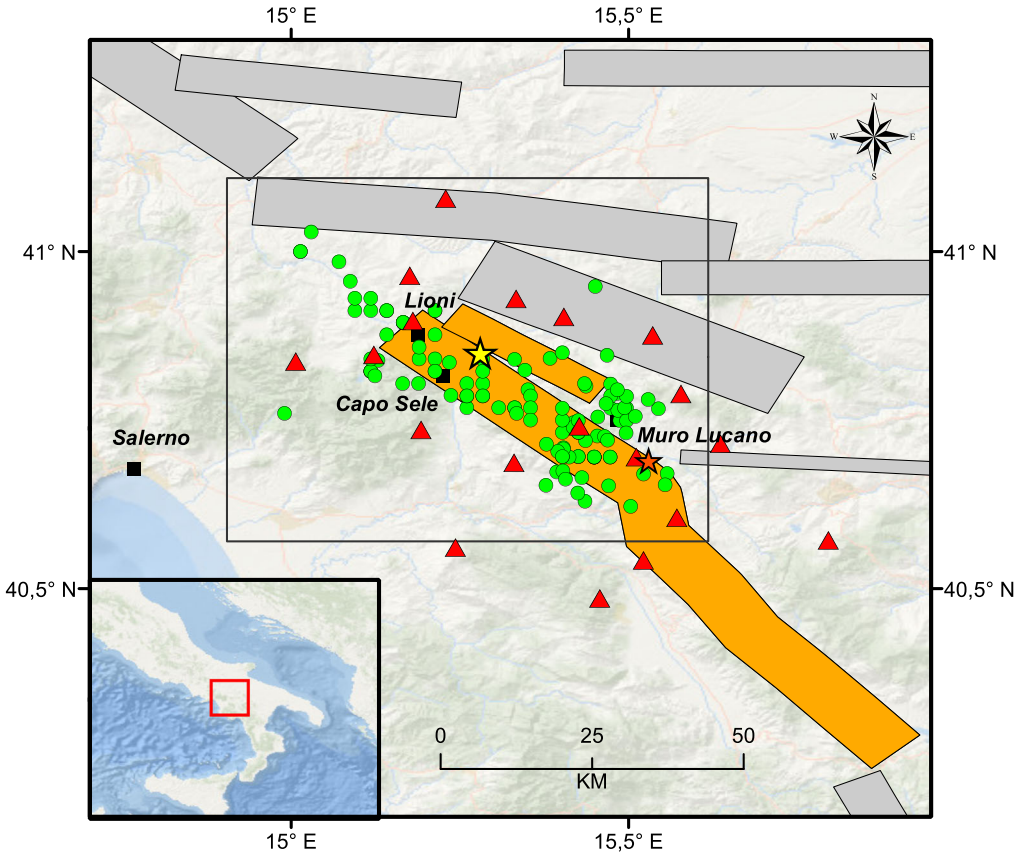

Fig. 1 Epicentral map of the earthquakes analysed in this study. Green circles refer to microseismicity recorded by Irpinia Seismic Network (ISNet, red triangles) during the year 2018 that falls within the explored area. This area, indicated by the black square, corresponds to the location of volumetric grid of potential hypocenters investigated in this work. Earthquake locations are derived from ISNet catalogue. Yellow star refers to the epicentral location of the November 23rd, 1980, M_s 6.9, Irpinia earthquake; while the orange star refers to the epicentral location of April 3rd, 1996, M_L 4.9 earthquake. Seismogenic sources related to Irpinia fault system are indicated in orange; potential sources for earthquakes larger than M 5.5 of surrounding areas are indicated in grey (Database of Individual Seismogenic Sources, DISS, Version 3.2.1 2018)

ISNet Bulletin web-page (http://isnet-bulletin.fisica.unina.it/cgi-bin/isnet-events/isnet.cgi). Since 2008, an average of about 260 earthquakes per year have been detected, with magnitudes (M_L) spanning the range between 0.1 and 3.3, and located within the area covered by the seismic network (173 earthquakes during the 2018), resulting in a seismic catalogue complete down to M_L 1–1.5, varying with time as the network evolved (Stabile et al. 2013).

For our analysis, we focus on an area of 3600 km^2 with the highest seismicity rate (Stabile et al. 2012), which corresponds to the epicentral zone of the M_s 6.9, 1980 Irpinia earthquake. For this area of study and the year 2018, a catalogue of 115 events with magnitude of completeness, M_c equal to 1, is available.

3 Method

We adopted a migration-based approach for detecting and locating earthquakes that exploits coherent (P- and S-wave) arrivals at different stations for an assumed 3D grid of potential source locations (Matos et al. 2016; Lopez-Comino et al. 2017; Adinolfi et al. 2019). To this goal, we used a recently developed detection and location algorithm (Lassie, https://gitext.gfz-potsdam.de/heimann/lassie, Heimann et al. 2017).

The processing includes the following steps (shown also in Fig. 2):

1) *Pre-processing*. Continuous waveforms are filtered in the frequency band of 1–15 Hz and cut in 20 min long

time windows with 20% of overlap, which in turn are used to compute characteristic functions (CFs). These latter are derived from the three-component recordings that are squared and combined by summation into a single trace, which is proportional to the seismic energy and it is smoothed by a convolution with a Hann window (i.e., we used a length of 10 s). To detect different seismic patterns and/or seismic phases (P- and S- waves) from the waveforms, in this study we worked with two CFs pre-processing schemes. In particular, we used two different CFs and travel time corrections for their shifting and stacking (described at step 2) for P- and S- wave packets, which results in two distinct Image Function Contributions (IFCs). For the P-IFC, a short-time average over long-time average (STA/LTA) trace, sensitive to sharp onsets of the seismic signal, is calculated using a short-time window length of 0.7 s and a long one of 1.0 s, as in Grigoli et al. (2013). For the S-IFC, the signal is normalized by its moving average of length 50 s. This processing results in a smooth positive CF for each station, which is sensitive to transient increases of seismic energy. The P-IFC and S-IFC images can be used individually (S-IFC in the step 2) or together (step 3) combined using summation, so as to form a final Global Image Function (GIF) that is effectively used for earthquakes detection. This pre-processing results in CFs used for calculating the IFCs in the next steps (2 and 3).

2) *Earthquake detection with S-wave.* The earthquake detection is performed defining a 3D grid of potential source locations with a size of 60 × 60 × 20 km (2 km grid spacing). Then, for each grid-node, the S-waves travel times were computed for all the seismic stations using a local 1D velocity model (Matrullo et al. 2013) using the CAKE tool (Heimann et al. 2017). For all the nodes of the 3D grid, the CFs are shifted in time according to their travel-times and stacked to form a so-called image function contribution (S-IFC). Therefore, the resultant S-IFC corresponds to a GIF that can be considered an indirect measure of signals coherence. Next, a novel time series of GIF is built by considering for each time step the highest coherence value in the spatial grid. Hence, the earthquake detection is performed by searching for local maxima in the GIF, whereas an event is declared whenever the GIF is greater than a selected threshold value. Adinolfi et al. (2019) observed that using only the S-waves to build the GIF images, with respect to using only the P-wave IFC or combining P- and S- wave IFCs, provided more robust results for the earthquake detection, but at the expense of a more uncertain location.

3) *Earthquakes' location with P- and S-waves*. Once the seismic events are declared, aiming to improve the event location estimates, steps 1 and 2 are repeated considering both P- and S-waves. Clearly, the P- and S-IFCs are derived by shifting in time the CFs according to the travel-times of the seismic waves for which are computed. Therefore, the IFCs proportional to P- and S-wave packet energies are equally weighted and stacked. Finally, the GIF is used to refine the earthquakes location.

4) *Discrimination between real and false detections.* High IFC values (hereinafter, we will use also 'high coherence values' for the sake of using a term familiar for seismologists) can be potentially attributed to both the arrival of coherent seismic energy at more seismic stations and a high signal-to-noise ratio. Several factors, as for instance network geometry, number of stations, noise conditions and earthquakes depth as well as magnitude, can influence the range of coherence values associated to the events. For this reason, the coherence value used as detection threshold for discriminating between real and false detections is generally manually defined.

In this study, we tuned the Lassie code to optimize both the real versus false events discrimination and the location, with the aim to improve its performance with respect to cases when a simple threshold criterion is adopted. In particular, we defined as 'triggered' seismic stations having an S-wave CF amplitude greater or equal than the average CF value computed for all stations. Indeed, triggered stations correspond to those mostly contributing to the stack of CFs and in determining the final coherence value associated to a seismic event. As expected, in case of the earthquake detection task, we observed that seismic stations located close to the epicentre are associated to larger S-wave CF amplitudes than those at greater distance (Fig. 2b and f). Therefore, the information concerning the 'triggered' stations allowed us to set a proximity criterion (as described further in more detail) for the real versus false event classification, which is based on inspecting if triggered stations correspond to those located closer to the estimated epicentre.

5) *Magnitude estimation.* Once an earthquake detection is classified as real, the local magnitude is estimated following Bobbio et al. (2009).

Two examples of high- and low-coherence detections are reported in Fig. 3. These examples refer to a M_L 3.3 earthquake occurred on the 2018-04-06 at 01:22:38.00 (UTC) nearby the Muro Lucano village and to a $M_L - 0.8$ earthquake occurred on the 2018-12-28 at 18:45:10.00 (UTC) nearby the Caposele village (Fig. 1).

In order to assess the performance of the coherence-based method with respect to the standard monitoring procedures applied at ISNet, we have followed the described multistep procedure, and we have adopted two different criteria for the selection of real and false events.

The first criterion is based on a classic threshold approach (*thrc*), for which a detection is considered as a real event by simply checking if its associated coherence exceeds the selected threshold. Aiming to recover the lowest possible magnitude events and to reduce the completeness magnitude of the catalogue, we have set the coherence threshold equal to 350, which corresponds to a coherence value (empirically evaluated) compatible with the ratio real/false detections observed at ISNet.

The second tested criterion combines the classic coherency threshold approach with a proximity rule based on the triggered stations (*tapc*) and a measure of coherency among the signal envelopes of triggered stations. Therefore, a detection is considered real when one of these two conditions is fulfilled: (1) when the detection is associated to a coherence value greater than 400, which is associated to larger magnitude events; (2) for detections associated to smaller coherence values than 400, we analyse the spatial distribution of triggered stations with respect to the not-triggered ones. Therefore, the detection is classified as real if among the three stations closest to the epicentre two are classified as triggered. After that, a set of detections according to the triggered stations' criterion is defined; a further analysis is performed to check the similarity of the signal envelopes. We performed this similarity check by implementing a cluster analysis where all the triggered seismic stations are considered. The aim of this final step is to identify, within the whole set of

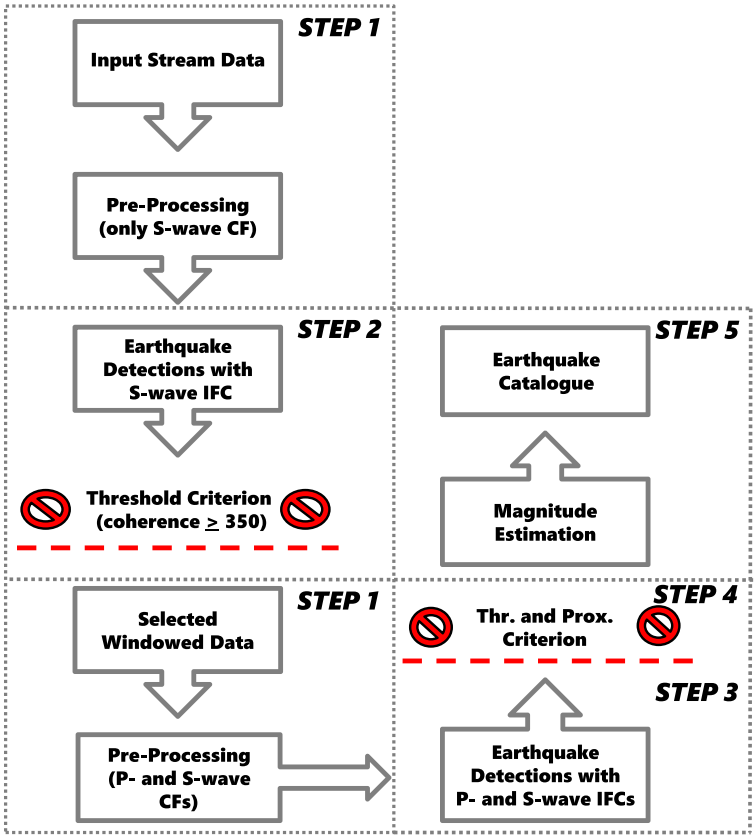

Fig. 2 Workflow of the multistep procedure for earthquake detection applied in this study

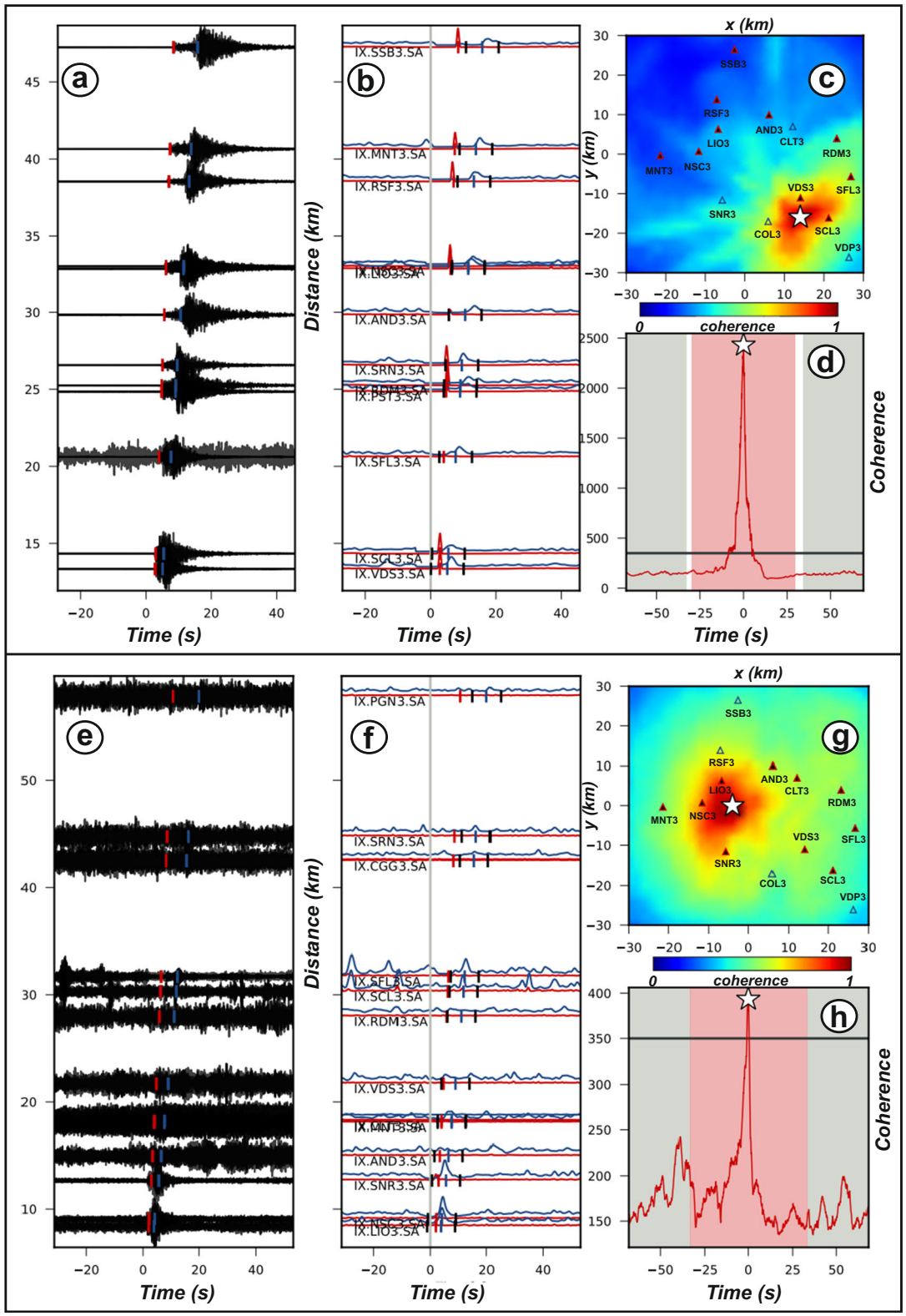
a
b
c
d
e
f
g
h
Distance (km)
Time (s)
x (km)
y (km)
coherence
Coherence
IX.SSB3.SA
IX.MNT3.SA
IX.RSF3.SA
IX.LIO3.SA
IX.AND3.SA
IX.SRN3.SA
IX.PST3.SA
IX.SFL3.SA
IX.SCL3.SA
IX.VDS3.SA
IX.PGN3.SA
IX.CGG3.SA
IX.RDM3.SA
IX.NSC3.SA
SSB3
RSF3
AND3
CLT3
LIO3
RDM3
MNT3
NSC3
VDS3
SFL3
SNR3
COL3
SCL3
VDP3

◀ **Fig. 3** Examples of high-coherence (**a**–**d**) and low-coherence (**e**–**h**) detections. **a**–**d** refer to the M_L 3.3 earthquake occurred on the 2018-04-06 at 01:22:38.00 (UTC) nearby the Muro Lucano village. **e**–**h** refer to the $M_L - 0.8$ earthquake occurred on the 2018-12-28 at 18:45:10.00 (UTC) nearby the Caposele village. **a**, **e** Waveforms used for detections are sorted by hypocentral distance. **b**–**f** Characteristic functions (normalized amplitude) calculated for each station. They are corrected according to the P-wave velocity (red lines) and S-wave velocity (blue lines) for the travel time and stacked to obtain the final global image function (**d**–**h**). The markers indicate the best fit of synthetic arrival time for P- and S- phases. Black markers indicate the time window over which the CF amplitude is considered for the definition of triggered or not-triggered stations. **c**–**g** Stack of the coherence map for the search region with available (red triangles), not-available seismic stations (blank triangles) and event detected (white star). The colour bar shows coherence values. **d**–**h** Global image functions corresponding to the best fit of source position along a processing time window centred on the origin time of the detected earthquake. The white star indicates the detected event above a fixed threshold value (black line)

detections, those with highly coherent signals. The similarity between envelopes is evaluated by cross-correlation, whose value is used to build the hierarchical cluster tree with the 'single linkage algorithm' (Johnson 1967). This agglomerative (iterative merging) method adopts for calculating the distance between two clusters the shortest distance between all pairs of the clusters. The hierarchical clustering is performed using a small distance threshold (equal to 1.25) in order to be more selective and robust in discriminating similar signals.

In conclusion, detections associated to clustered stations with highly similar envelopes are accepted as real events, while those generated by isolated stations or not belonging to any cluster are discharged. The tuning of the parameters (i.e., coherence threshold, number of stations for the proximity rule, and for the cluster analysis) selected for the *thrc* and *tapc* criteria has been carried out considering 2 months of data (May–June 2018), which have been used as training dataset. The tuning has been performed considering the earthquake detections classified as real or false by the visual inspection of waveforms. The coherence values set as threshold for *thrc* and *tapc* have been defined considering the data in the ISNet catalogue. In particular, a threshold equal to 400 corresponds to a high real/false detection ratio consistent with the occurrence of larger magnitude events, while the value of 350 allows to detect smaller magnitude events but can fail to discriminate real from false detections.

4 Results

Applying the detection criteria *thrc* and *tapc* results in an increased number of detected events (i.e., 322 events and 198, respectively) in comparison with the manually revised events in the ISNet earthquake catalogue (115 events).

To carry out a preliminary performance analysis of the two criteria, we used the 2 months training set of data (May–June 2018), and for both the criteria, all the detections were visually inspected. During these 2 months, we found 69 detections with 41 real events considering *thrc* and 51 detections with 39 real events using *tapc*. Hence, using *thrc*, we observe a little improvement (two events) with respect to applying *tapc*, but at the cost of an increase in false detections (i.e., equal to 16). Using the *tapc* criteria results in a percentage of success (number of real detections divided by the number of total detections) equal to 76.5%, while using *thrc*, the percentage of success is 59.4%. We observe that the detection of weak signals is achieved at the cost of increasing the number of false detections, which have been generated by seismic noise sources related to environment conditions or human activities. The *tapc* criterion allows obtaining low number of false detections assuring a high rate of success, and thus, in our opinion, it can be very useful for detecting small magnitude earthquakes associated to low-coherence values.

We used the *tapc* criteria for analysing the 1-year long dataset. To assess the performance of the detector algorithm, we visually inspected the waveforms of all the detections, and we found 152 real earthquakes and 46 false detections. In contrast, the ISNet catalogue for the same period consists of 115 manually detected and located events. Therefore, the automatic *tapc* criterion allowed us to identify 37 new earthquakes with respect to the manual ISNet catalogue. It is worth noting that doing a comparison with the automatic Earth-worm Binder (Dietz 2002) implemented in ISNet, the better performance of the *tapc* detector is even more evident. The number of automatically detected by Earth-worm Binder events at ISNet are 44 with respect to the 152 found by *tapc* (See Supplementary Material).

Our results confirm that an event-discrimination strategy based only on a coherence threshold is not optimal for discriminating real and false events. In fact, it would force the operators to find a difficult compromise between the need of detecting earthquakes with the lowest possible magnitude and the need of avoiding the corruption of earthquake catalogues with false

detections. Our strategy (i.e., the *tapc* criterion), which combines coherence information, event locations, and signal characteristics of the triggered stations, allows improving by 245.4% and 32.2% the performance of the event detection in comparison to the automatic and manual proceedings used for building the ISNet catalogue, respectively. The frequency-magnitude distributions (Gutenberg and Richter 1942; Aki 1965; Wiemer 2001) obtained considering the *tapc* detection is shown in Fig. 4 in comparison with the one from the manual catalogue of ISNet for the same area and period. The *tapc* catalogue shows an increase of earthquake detections and a decrease in the completeness magnitude M_c to M_L equal to 0.5, but without adding a significant number of false events. In comparison, the ISNet catalogue is complete for magnitude M_L around 1 (Fig. 4).

Despite the good detection performance, it is worth noting that the automatic detections algorithm missed 46 earthquakes, with magnitude ranging between M_L 0.4 and M_L 3 (i.e., among them only one has M_L 3) which instead were found in the ISNet catalogue (See Supplementary Material). Of these missed events, 19 earthquakes have $M_L \geq 1$, while 27 have $M_L \leq 1$. However, we found that only 4 earthquakes have $M_L \geq 1.5$ and, most important, they are located near the border of the explored area (Supplementary Material, Fig. S1 and S2). Furthermore, of these missed earthquakes, the two events with M_L 2.8 and M_L 3 show a difference in origin time of about 4 s only. The concurrence of these two earthquakes resulted in an anomalous, broad double-peaks in the CF, which were in turn incorrectly stacked into a biased GIF not exceeding the chosen threshold (Supplementary Material, Fig. S3). We note, however, that also in this peculiar case setting a lower value of coherence (200), the M_L 3 earthquake can be detected. Concerning the 27 earthquakes with $M_L \leq 1$, 10 events occurred at a depth larger than 10 km, 8 events had hypocentral depth between 5 and 10 km, while the other 9 events occurred at depth smaller than 5 km. Also, we observed that by lowering the coherence value to 180, these events can be detected.

We therefore found different reasons why these 46 earthquakes could have been missed: (1) Low magnitude events ($M_L < 1$) have not been detected because their coherence values are smaller than the selected

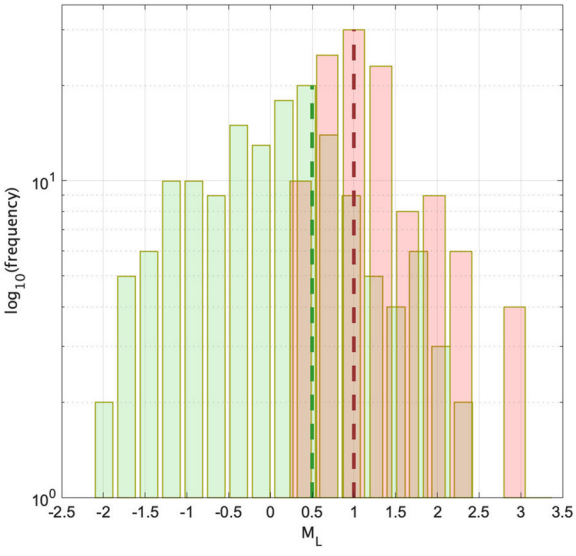

Fig. 4 Frequency-magnitude distribution for the ISNet catalogue (red bars, and completeness magnitude M_c as red dashed line) and for the earthquakes catalogue derived in this study using the *tapc* criterion (green bars, and M_c as green dashed line)

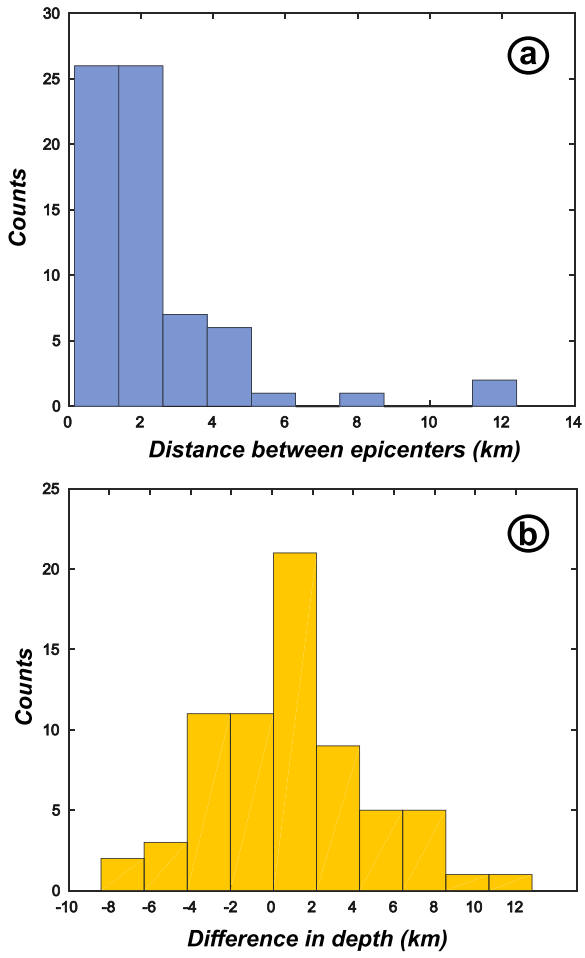

Fig. 5 Histograms of the distance between epicentres (**a**) and of the difference in depth (**b**) for the earthquake locations calculated in this study and those derived by the ISNet catalogue

threshold. Clearly, these events could eventually be identified selecting a lower threshold for the coherence, but at the cost of increasing the number of false detections. (2) Similarly, deep earthquakes, that is to say events with hypocentral depth larger than 10 km, have been missed likely because they are characterized by too small S-wave amplitudes, which led the final GIF to not exceed the selected coherency threshold. Since shallow seismicity is our main objective, we will investigate the best set of parameters for the detection of deep earthquakes in the future work. (3) We observed that changes in the operating conditions of the local seismic network, especially changes in the number of functioning seismic stations, have a strong impact on the detector performance. Indeed, once a threshold of coherence is fixed, decreasing the number of stations results in a decrease of the number of detected seismic events and the increase of missed events. (4) The seismicity occurring at the borders of the explored area is not correctly identified due to the location errors. In fact, events located near the borders are likely to be mislocated outside of the explored grid, and consequently, are not correctly detected. Enlarging the explored area and using a more dense grid spacing could be sufficient to reduce the location errors and to solve this kind of problem, but at the cost of longer computational times.

We achieved reliable earthquake locations, as shown by the comparison of our results with the locations of ISNet manually revised catalogue (http://isnet-bulletin.fisica.unina.it/cgi-bin/isnet-events/isnet.cgi; Fig. 5). For the common events at the two datasets, most locations differ by less than 2 km both in terms of epicentre and depth (i.e., a value in agreement with the adopted 2 km grid spacing). As shown in Fig. 6, the retrieved earthquake locations show a clustering near the epicentral area of the M_s 6.9, 1980 Irpinia earthquake

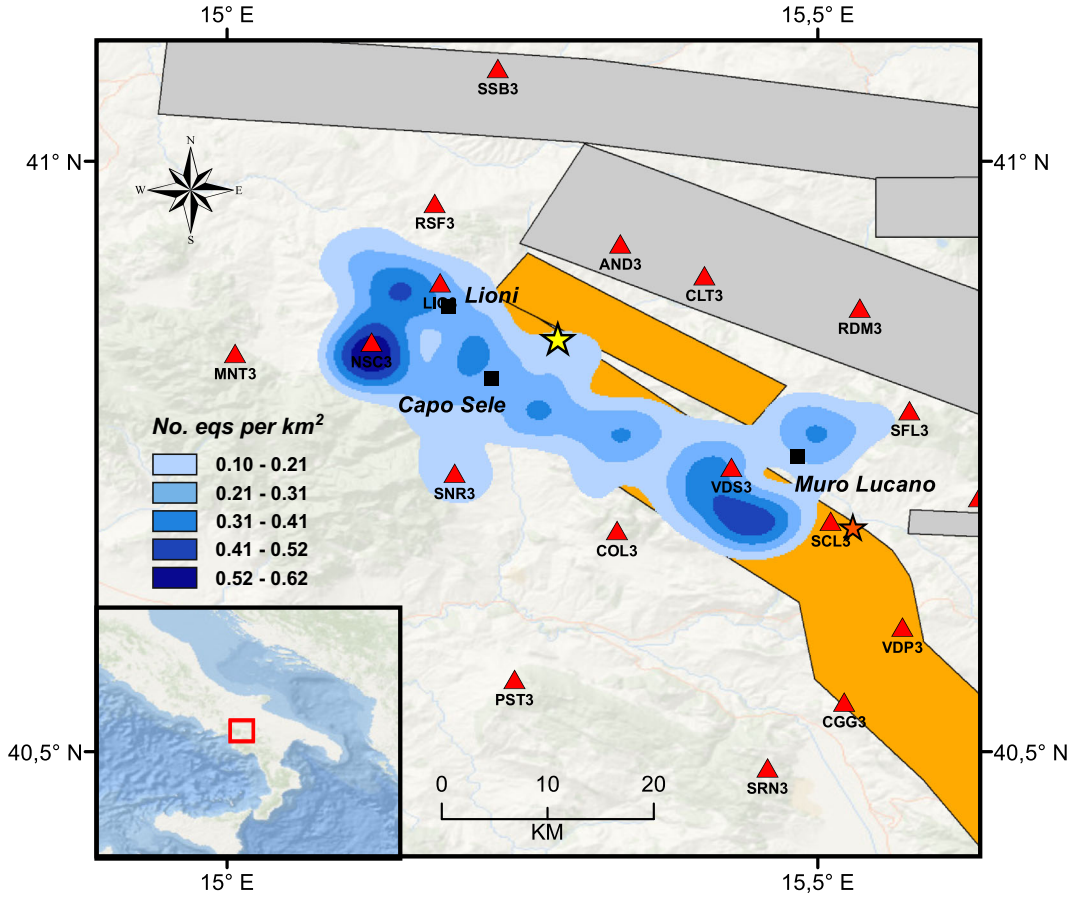

Fig. 6 Map showing the density of the earthquake locations calculated in this study using both P- and S-wave contributions. The earthquake detections are selected automatically using both threshold and proximity criteria. Contouring of the earthquakes per unit area (1 km^2) is indicated in blue. For more information, see Fig. 1

and a preferential NW-SE trend, in agreement with the orientation of active fault structures.

The automatic detection procedure resulted to be very fast. Indeed, 1 year of data recorded at 19 three-component seismic stations and the scanning of a volume grid made by 9000 nodes were processed within about 1.75 days using a multiprocessor personal computer (Intel® Core™ i5–7500 CPU @ 3.40GHz × 4, 8 GiB RAM, Ubuntu 17.10 64-bit).

5 Conclusions

One-year of seismic data recorded at a near-fault observatory along the Irpinia fault zone were analysed with a coherence-based method for earthquake detection. An automated, fast, multistep procedure was applied as new strategy to discriminate real/false detections and to locate earthquakes. An increase in the number of automatic earthquake detections compared to the ISNet catalogues was obtained, showing a decrease in completeness magnitude of about 0.5 units. The earthquakes catalogue retrieved by the multistep procedure is complete down to M_L 0.5. Although special attention must be paid for identifying earthquakes that could occur at larger depths or at border of the explored area, our strategy resulted to be able to improve approximately by 245% and 32% the automatically and manually detected events in the reference catalogue, respectively. Our results show that fast and automated methods for the detection and location of microseismicity, as the coherence-based applied in this study, represent a valid tool to process large dataset, to monitor natural/induced seismicity and to achieve a more complete seismic catalogue.

Acknowledgments We thank the Editor T. A. Stabile and three anonymous reviewers for their comments which helped us in improving the manuscript. This work has been supported by the Italian Ministry for Economic Development (MiSE), Directorate-General for Mineral and Energy Resources, within a program agreement with the University of Naples "Federico II."

References

Adinolfi GM, De Matteis R, Orefice A, Festa G, Zollo A, de Nardis R, Lavecchia G (2015) The September 27, 2012, ML 4.1, Benevento earthquake: a case of strike-slip faulting in southern Apennines (Italy). Tectonophysics 660:35–46. https://doi.org/10.1016/j.tecto.2015.06.036

Adinolfi GM, Cesca S, Picozzi M, Heimann S, Zollo A (2019) Detection of weak seismic sequences based on arrival time coherence and empiric network detectability: an application at a near fault observatory. Geophys J Int 218(3):2054–2065. https://doi.org/10.1093/gji/ggz248

Amoroso O, Russo G, De Landro G, Zollo A, Garambois S, Mazzoli S et al (2017) From velocity and attenuation tomography to rock physical modeling: inferences on fluid-driven earthquake processes at the Irpinia fault system in southern Italy. Geophys Res Lett 44(13):6752–6760. https://doi.org/10.1002/2016GL072346

Aki K (1965) Maximum likelihood estimate of b in the formula log N= a-bM and its confidence limits. Bull Earthq Res Inst, Tokyo Univ 43:237–239

Bernard P, Zollo A (1989) The Irpinia (Italy) 1980 earthquake: detailed analysis of a complex normal faulting. J Geophys Res Solid Earth 94(B2):1631–1647. https://doi.org/10.1029/JB094iB02p01631

Bobbio A, Vassallo M, Festa G (2009) Local magnitude estimation for the Irpinia seismic network. Bull Seismol Soc Am 99:2461–2470. https://doi.org/10.1785/0120080364

Cesca S, & Grigoli F (2015) Full waveform seismological advances for microseismic monitoring. In *Advances in Geophysics*(Vol. 56, pp. 169-228). Elsevier https://doi.org/10.1016/bs.agph.2014.12.002

Cocco M, Chiarabba C, Di Bona M, Selvaggi G, Margheriti L, Frepoli A et al (1999) The April 1996 Irpinia seismic sequence: evidence for fault interaction. J Seismol 3(1):105–117. https://doi.org/10.1023/A:1009771817737

De Landro G, Amoroso O, Stabile TA, Matrullo E, Lomax A, Zollo A (2015) High-precision differential earthquake location in 3-D models: evidence for a rheological barrier controlling the microseismicity at the Irpinia fault zone in southern Apennines. Geophys J Int 203(3):1821–1831. https://doi.org/10.1093/gji/ggv397

De Matteis R, Matrullo E, Rivera L, Stabile TA, Pasquale G, Zollo A (2012) Fault delineation and regional stress direction from the analysis of background microseismicity in the southern Apennines, Italy. Bull Seismol Soc Am 102(4):1899–1907. https://doi.org/10.1785/0120110225

Dietz L (2002) Notes on configuring binder_ew: Earthworm's phase associator

DISS Working group (2018) Database of individual seismogenic sources (DISS), version 3.2.1: a compilation of potential sources for earthquakes larger than M 5.5 in Italy and surrounding areas. http://diss.rm.ingv.it/diss/, Istituto Nazionale di Geofisica e Vulcanologia; https://doi.org/10.6092/INGV.IT-DISS3.2.1

Ekström G (2006) Global detection and location of seismic sources by using surface waves. Bull Seismol Soc Am 96(4A):1201–1212. https://doi.org/10.1785/0120050175

Gajewski D, Tessmer E (2005) Reverse modelling for seismic event characterization. Geophys J Int 163(1):276–284. https://doi.org/10.1111/j.1365-246X.2005.02732.x

Gharti HN, Oye V, Roth M, Kühn D (2010) Automated microearthquake location using envelope stacking and robust global optimization automated microearthquake location.

Geophysics 75(4):MA27–MA46. https://doi.org/10.1190/1.3432784

Grigoli F, Cesca S, Amoroso O, Emolo A, Zollo A, Dahm T (2013) Automated seismic event location by waveform coherence analysis. Geophys J Int 196(3):1742–1753. https://doi.org/10.1093/gji/ggt477

Grigoli F, Scarabello L, Böse M, Weber B, Wiemer S, Clinton JF (2018) Pick-and waveform-based techniques for real-time detection of induced seismicity. Geophys J Int 213(2):868–884. https://doi.org/10.1093/gji/ggy019

Gutenberg B, Richter CF (1942) Earthquake magnitude, intensity, energy, and acceleration. Bull Seismol Soc Am 32(3):163–191

Heimann S, Kriegerowski M, Isken M, Cesca S, Daout S, Grigoli F, Juretzek C, Megies T, Nooshiri N, Steinberg A, Sudhaus H, Vasyura-Bathke H, Willey T, Dahm T (2017) Pyrocko - an open-source seismology toolbox and library. *GFZ Data Services*, Potsdam. https://doi.org/10.5880/GFZ.2.1.2017.001

Johnson SC (1967) Hierarchical clustering schemes. Psychometrika 32(3):241–254. https://doi.org/10.1007/BF02289588

Kao H, Shan SJ (2007) Rapid identification of earthquake rupture plane using source-scanning algorithm. Geophys J Int 168(3):1011–1020. https://doi.org/10.1111/j.1365-246X.2006.03271.x

Klein FW (2003) The HYPOINVERSE2000 earthquake location program. Int Geophys 81:1619–1620. https://doi.org/10.1016/S0074-6142(03)80287-5

Krüger F, Ohrnberger M (2005) Tracking the rupture of the M w= 9.3 Sumatra earthquake over 1,150 km at teleseismic distance. Nature 435(7044):937. https://doi.org/10.1038/nature03696

López-Comino JA, Cesca S, Heimann S, Grigoli F, Milkereit C, Dahm T, Zang A (2017) Characterization of hydraulic fractures growth during the Äspö hard rock laboratory experiment (Sweden). Rock Mech Rock Eng 50(11):2985–3001. https://doi.org/10.1007/s00603-017-1285-0

Matos C, Heimann S, Grigoli F, Cesca S, & Custódio S (2016) Seismicity of a slow deforming environment: Alentejo, South Portugal. In *EGU General Assembly Conference Abstracts*(Vol. 18, p. 278)

Matrullo E, De Matteis R, Satriano C, Amoroso O, Zollo A (2013) An improved 1-D seismic velocity model for seismological studies in the Campania–Lucania region (southern Italy). Geophys J Int 195(1):460–473. https://doi.org/10.1093/gji/ggt224

McMechan GA (1982) Determination of source parameters by wavefield extrapolation. Geophys J Int 71(3):613–628. https://doi.org/10.1111/j.1365-246X.1982.tb02788.x

Maercklin N, Festa G, Colombelli S, Zollo A (2012) Twin ruptures grew to build up the giant 2011 Tohoku, Japan, earthquake. Sci Rep 2:709. https://doi.org/10.1038/srep00709

Picozzi M, Bindi D, Zollo A, Festa G, Spallarossa D (2019) Detecting long-lasting transients of earthquake activity on a fault system by monitoring apparent stress, ground motion and clustering. Sci Rep 9:16268–16211. https://doi.org/10.1038/s41598-019-52756-8

Rubinstein JL, Beroza GC (2007) Full waveform earthquake location: application to seismic streaks on the Calaveras fault, California. J Geophys Res Solid Earth 112(B5). https://doi.org/10.1029/2006JB004463

Stabile TA, Iannaccone G, Zollo A, Lomax A, Ferulano MF, Vetri MLV, Barzaghi LP (2013) A comprehensive approach for evaluating network performance in surface and borehole seismic monitoring. Geophys J Int 192(2):793–806. https://doi.org/10.1093/gji/ggs049

Stabile TA, Satriano C, Orefice A, Festa G, & Zollo A (2012) Anatomy of a microearthquake sequence on an active normal fault. *Scientific reports, 2*(1), Art N 410, 1–7. https://doi.org/10.1038/srep00410

Wassermann J (1997) Locating the sources of volcanic explosions and volcanic tremor at Stromboli volcano (Italy) using beam-forming on diffraction hyperboloids. Phys Earth Planet Inter 104(1–3):271–281. https://doi.org/10.1016/S0031-9201(97)00041-1

Weber E, Iannaccone G, Zollo A, Bobbio A, Cantore L, Corciulo M et al (2007) Development and testing of an advanced monitoring infrastructure (ISNet) for seismic early-warning applications in the Campania region of southern Italy, In *Earthquake Early Warning Systems* (pp. 325–341). Springer, Berlin, Heidelberg. https://doi.org/10.1007/978-3-540-72241-0_16

Wiemer S (2001) A software package to analyze seismicity: ZMAP. Seismol Res Lett 72(3):373–382. https://doi.org/10.1785/gssrl.72.3.373

Withers M, Aster R, Young C (1999) An automated local and regional seismic event detection and location system using waveform correlation. Bull Seismol Soc Am 89(3):657–669

Zeng X, Zhang H, Zhang X, Wang H, Zhang Y, Liu Q (2014) Surface microseismic monitoring of hydraulic fracturing of a shale-gas reservoir using short-period and broadband seismic sensors. Seismol Res Lett 85(3):668–677. https://doi.org/10.1785/0220130197